Hysteresis Compensation Application in Magnetostrictive Inkjet Print-head

Tran Quoc Bao

Faculty of Mechatronics, School of Mechanical and Automotive Engineering, Hanoi University of Industry, Vietnam

baotq@haui.edu.vn (corresponding author)

ABSTRACT

This study presents the experimental hysteresis compensation method implemented in a magnetostrictive inkjet print-head, utilizing the Terfenol-D, a giant magnetostrictive material. The distinctive features between the input energy and the output displacement are known as the inherent hysteresis characteristics in a ferromagnetic material, which cause major obstacles to the output performance. Therefore, an appropriate compensation method is necessary to reduce the Hysteresis Loss (HL). Previous research has focused on mathematical models such as the Preisach or the Jile – Atherton models. However, such models are complicated, and it is thus challenging for them to control hysteresis in a real-time system. This paper solves the aforementioned problem based on the charging and discharging of an RC-circuit, which is known as the experimental compensation method. In the experiment, an attempt to compensate for hysteresis at the frequencies of 5 Hz and 100 Hz is made. For each frequency, different ranges of the capacitance value are selected to find the resistance value. A resistor with the value of 50 Ω is chosen and integrated into the compensation circuit. Through the experiment, optimal capacitance values of 335 μF and 10.75 μF are obtained at the considered frequencies. The results are attained using PEDOT: PSS and silver nanoparticle ink to validate the droplet formation. In both cases, the droplet formation is estimated and calculated in terms of the droplet diameter, tail length, droplet volume, and breaking time.

Keywords-magnetostrictive actuator; inkjet technology; hysteresis compensation

I. INTRODUCTION

The inkjet printing technology has been developing for decades and has become prevalent in various industries. It can be categorized into two particular groups, namely, Continuous Inkjet Technology (CIJ) and Drop-on-Demand Inkjet Technology (DoD) [1-3]. In CIJ, the droplet formation is created by applying the vibration from a piezoelectric crystal. A pressure wave passes through the nozzle, the ink flows, and is divided into equal sizes at a certain range of space [4]. Many drops are charged by the vibration and are simultaneously printed onto the substrate in a multiple defluxion system, while the uncharged drops fly back to the gutter for recirculation. In DoD, four types of inkjet printing technology are included, namely thermal, piezoelectric, electrostatic, and acoustic [5]. The DoD technology has becomes more popular compared to CIJ, especially in electronic printing applications and low-cost printings [6-7]. The inkjet printing technology faces challenges, particularly when working with high-viscosity fluids that impact the droplet formation and ejection consistency. Authors in [8] discovered a new actuation waveform that can be used with single-drop and multi-drop ejection techniques. In [9], a high-viscosity liquid was utilized with a magnetostrictive inkjet print-head, proving that the pouring of such a liquid is feasible. In [10], where the jet stability method was investigated, more uniform designs were developed. Authors in [11] discussed the development of a new electrode configuration for an electrostatic inkjet printing head. Aiming to improve resolution in micro-displays for the Augmented Reality (AR) and Virtual Reality (VR) technologies, authors in [12] examined various inkjet printing techniques, such as aerosol, piezoelectric, and electro-hydrodynamic printing, and how they can help overcome issues, like coffee-ring effects and ink optimization. These techniques' implementation in wearable, flexible electronics is becoming the cutting edge of portable health monitoring, human–machine interface, and other electronic and optical applications [13]. The ink properties were demonstrated in [14] combined with a printing strategy, making sensor devices more flexible and wearable at present and in the future [15].

The magnetostrictive inkjet technology is a highly advanced and precise method of inkjet printing, which is especially well-suited for applications where traditional piezoelectric or thermal inkjet technologies may fail to meet performance requirements [16]. Authors in [17] presented the capability of high frequency driving, while strong output forces were used by a magnetostrictive actuator to produce relatively large displacements in comparison to other upcoming actuator technologies. Authors in [18] focused on the dynamic of a magnetostrictive actuator, having applied the prestress effect to verify hysteresis loop. In order to achieve accurate and reliable droplet ejection in magnetostrictive inkjet print-heads, some methods have been exploited to mitigate the effect of

hysteresis. Hysteresis compensation combines modeling, control schemes, and adaptive approaches [19-21]. These techniques are vital for preserving dependability and excellent print quality in situations where accuracy is crucial. A smart actuator, such as Terfenol-D, has been utilized in magnetostrictive inkjet showing strong force, yet displaying a significant hysteresis. Previous studies on hysteresis have deployed a state observer based on the Bouc–Wen model to estimate and compensate for hysteresis [22]. In [23], the nanopositioning systems were reviewed, which demonstrate periodic stability of the close loop system via comparison with the multiple inversion – based and inversion – free approach. In addition, a robust control strategy was introduced that effectively compensates for the hysteresis nonlinearity in nanopositioning systems, which is critical for high-precision applications, like atomic force microscopy and nanomanufacturing. Authors in [24] focused on improving the accuracy of hysteresis modeling and compensation for Piezoelectric Actuators (PEAs), particularly under high-frequency, and the results displayed complex signal conditions. Having used a combination of hysteresis inversion and sliding mode control, the proposed Adaptive Conditional Servocompensator (ACS) achieved superior tracking accuracy and robustness. To attain optimal performance in magnetostrictive inkjet printing systems, several techniques may be applied in practice, such as feedback control for fine-tuning and a feed-forward model for baseline compensation. Another example of linearizing the actuator response with inverse algorithms and creating mathematical models to describe hysteresis has been investigated in smart actuators, like magnetostrictive materials [25]. Some of the discussed methods to compensate for smart material hysteresis are effective but extremely complicated in calculation and computerization. Laminating Terfenol-D can reduce the eddy current loss, but it can also affect the material's characteristics.

The current study employs an experimental method to compensate for the hysteresis of Terfenol-D by using an RC-circuit. The hysteresis curve is analyzed at the frequencies of 5Hz and 100Hz. Subsequently, HL is calculated and the proposed model is implemented to inkjet the print-head system, and thus verify the droplet characteristics. At the frequency of 5 Hz with the optimal capacitance value of 335 µF, the HL accounts for 4.32% and the efficiency of hysteresis compensation (HE) reaches 79.55%. At 100 Hz, the optimal capacitance is determined to be 10.75, HL accounts for 16.62%, and the HE attains 58.53%. After the compensation with the determined RC-circuit, hysteresis compensation in Mag-Jet is employed for droplet formation at the frequencies of 5 Hz and 100 Hz.

II.   EXPERIMENTAL SETUP

The hysteresis compensation setup involves a magnetostrictive actuator, a power amplifier, a function generator, an RC-circuit, a capacitive sensor, an oscilloscope, an XYZ stage, a Z stage, a current probe, a computer with a data acquisition system, and an optical table. The actuator, covered by a permanent magnet, allows bi-directional movement. A function generator generates input waveforms for the RC-circuit. The XYZ stage has a groove for sensor cable

stability. The function generator produces triangular waveforms with a 50% symmetry setting. The triangular input waveform is set at 200 µs with a 5 Hz sampling rate and supply voltage at a ± 3.5 V peak-to-peak value. The output signal is amplified 10 times with a LPA5B power amplifier before being fed into a magnetostrictive actuator. Also a CapaNCDT sensor is mounted on the XYZ stage, as depicted in Figure 1.
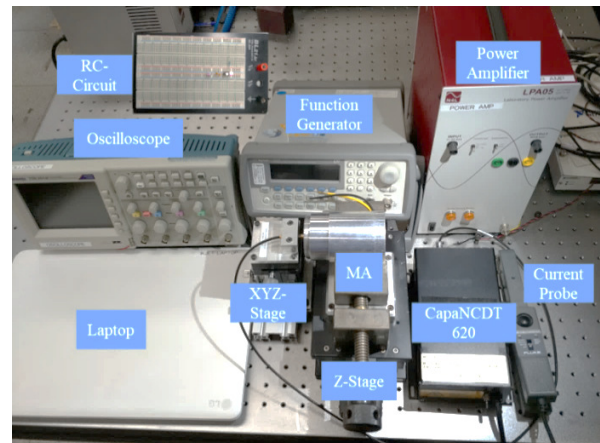

Fig. 1.   Experimental setup for hysteresis compensation.

The hysteresis loop at the frequency of 5 Hz with a selectively different capacitance is presented in Figure 2, where it is noticed that the loop decreased with higher capacitance values ranging from 108 µF to 335 µF. The optimized capacitor generated a current of ± 0.43 A with a displacement of 16.01 µm. The current dropped due to the greater energy storage during the capacitance charge and discharge.
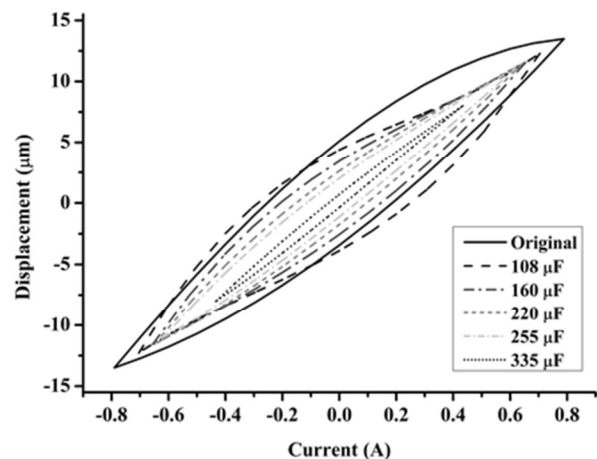

Fig. 2.   Hysteresis compensation at 5Hz.

Figure 3 presents the hysteresis characteristic for several capacitance values at a frequency of 100 Hz. The supply voltage is set up at ± 5V generating a displacement value of 25.16 µm in the original state. The optimal capacitance value of 10.75 µF results in a displacement of 18.05 µm and a current of approximately 0.7 A.
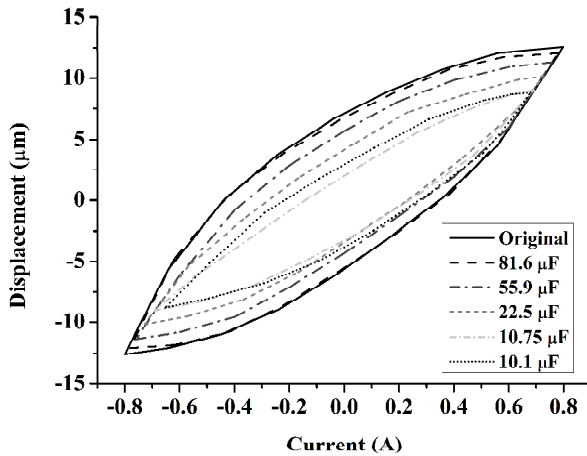
Fig. 3.   Hysteresis compensation at 100 Hz.

The hysteresis compensation method is deployed to evaluate the droplet formation on the magnetostrictive inkjet print-head. Figure 4 portrays the HL evaluation using the area of close loop between the rectangular reference area. The results are obtained utilizing PEDOT:PSS and silver nanoparticles based on synchronized triggering signals from a computer and a high-speed camera. HL constitutes an evaluation tool to assess the efficiency of hysteresis compensation, typically calculated by dividing the magnetic field strength (H) by the magnetic flux density (B).
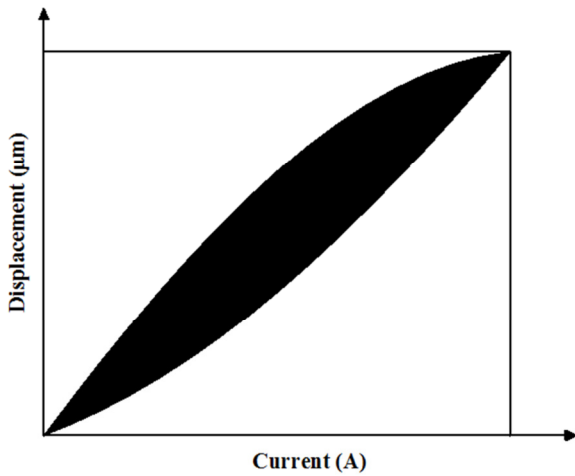

Fig. 4.   The hysteresis curve and rectangular reference.

The efficiency of the hysteresis compensation (HE) is calculated by:

$$HE = \frac{HL_{Original} - HL_{Capacitor}}{HL_{Original}} \times 100\% \qquad (1)$$

where $HL_{Original}$ and $HL_{Capacitor}$ are the HL without and with the RC-circuit, respectively.

HL is calculated by:

$$HL = \frac{A_{hysteresis}}{A_{Rectangular\ reference}} \times 100\% \qquad (2)$$

Table I presents five categories of processing, which include capacitance, current, displacement, HL, and HE. The frequencies of 5 Hz and 100 Hz are both used to evaluate the five categories' capacitance values and compare them with the original value.

TABLE I.   HL EVALUATION

Capacitance (μF)	Current (A)	Displacement (μm)	HL (%)	HE (%)
5 Hz				
0	-0.8 ~ 0.8	26.98	21.13	-
108	-0.8 ~ 0.8	24.58	22.5	6.48
160	-0.65 ~ 0.65	23.13	17.3	18.13
220	-0.62 ~ 0.62	23.23	12.63	40.23
255	-0.62 ~ 0.62	22.26	9.45	55.28
335	-0.43 ~ 0.43	16.01	4.32	79.55
100 Hz				
0	-0.8 ~ 0.8	25.16	40.08	-
10.10	-0.65 ~ 0.65	17.59	21.12	47.31
10.75	-0.7 ~ 0.7	18.05	16.62	58.53
22.5	-0.73 ~ 0.73	20.35	26.63	33.56
55.9	-0.76 ~ 0.76	22.66	31.03	22.6
81.6	-0.78 ~ 078	24.12	38.89	2.97

III.   RESULTS AND DISCUSSION

The experimental evaluation setup for droplet verification included a laptop connected with a high-speed camera and a magnetostrictive inkjet print-head mounted on 3D printing for tracking the droplet formation. An oscilloscope and a DAQ were used for signal acquisition. The entire experimental component was placed on an optical table.
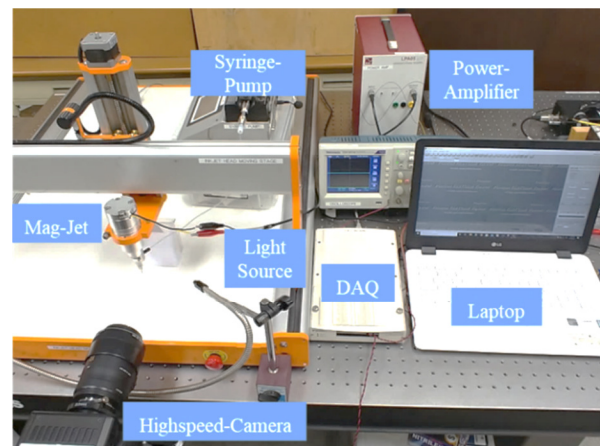

Fig. 5.   Experimental setup for droplet formation.

The procedure was performed with two different inks to compare the inkjet formation and characteristics. The experiment was carried out in two phases. In the first one, PEDOT:PSS and silver nanoparticle ink were utilized to validate the droplet formation at the frequency of 5 Hz before and after compensation. The experiment was conducted in a

laboratory at room temperature, and the capture of images by a high speed camera was reinforced with a light source. Figures 6 and 7 present the droplet formation before and after applying hysteresis compensation with PEDOT:PSS. Figures 8 and 9 illustrate the droplet generation while deploying silver nanoparticle ink. The droplet formation results show that the bubble ink is reduced after hysteresis compensation.
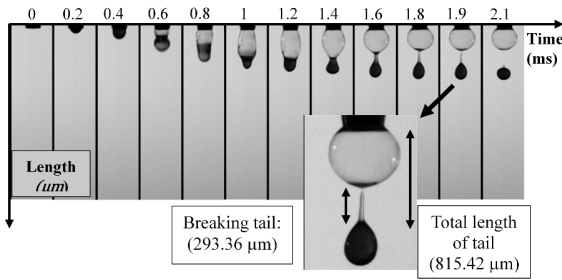

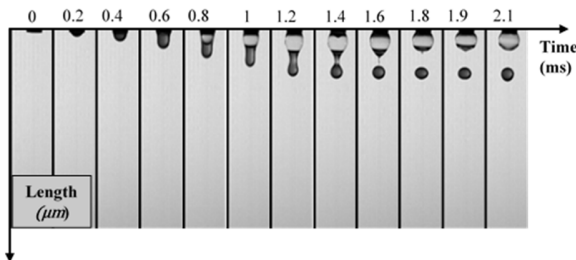Fig. 6.   Droplet formation at 5 Hz with PEDOT:PSS.

Fig. 7.   Droplet formation after hysteresis compensation at 5 Hz with PEDOT:PSS.
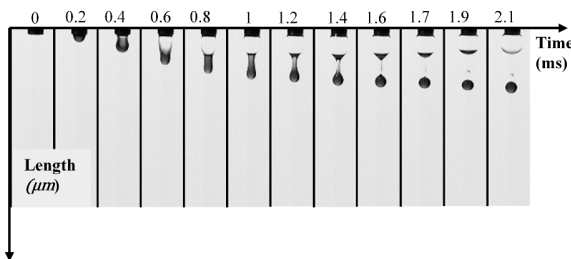

Fig. 8.   Droplet formation at 5 Hz with silver nanoparticle ink.

Table II summarizes the droplet formation evaluation at 5 Hz for both cases before and after compensation, with the recording time set from 0 to 2.1 ms.
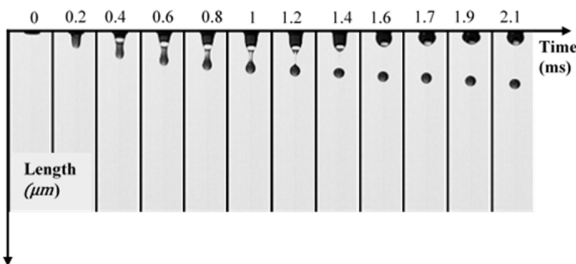

Fig. 9.   Droplet formation after hysteresis compensation at 5 Hz with silver nanoparticle ink.

TABLE II.   DROPLET FORMATION EVALUATION WITH PEDOT:PSS AND SILVER NANOPARTICLE INK AT 5 HZ.

Parameters	Before compensation	After compensation
PEDOT:PSS		
Droplet making time (ms)	1.85	1.55
Droplet diameter (µm)	277.5	263.34
Droplet volume (nL)	11.19	9.56
Breaking tail (µm)	293.36	146.48
Total tail (µm)	815.42	642.86
SILVER NANOPARTICLE INK		
Droplet making time (ms)	2.15	1.75
Droplet diameter (µm)	210.54	187.65
Droplet volume (nL)	4.89	3.46
Breaking tail (µm)	525.05	420
Total tail (µm)	885.39	877.5

In the second part of the experiment, PEDOT:PSS and silver nanoparticle ink were employed to validate the droplet formation at the frequency of 100 Hz before and after hysteresis compensation. Figures 10 and 11 present the droplet formation before and after applying hysteresis compensation with PEDOT:PSS at 100 Hz. Figures 12 and 13 display the droplet generation while deploying silver nanoparticle ink at 100 Hz.
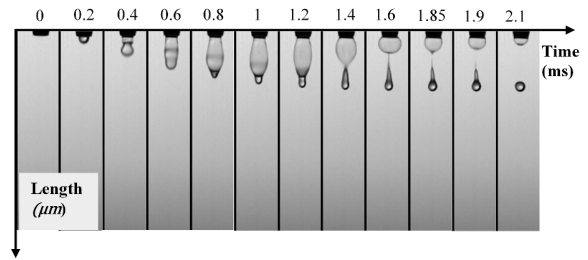

Fig. 10.   Droplet formation at 100 Hz with PEDOT:PSS.
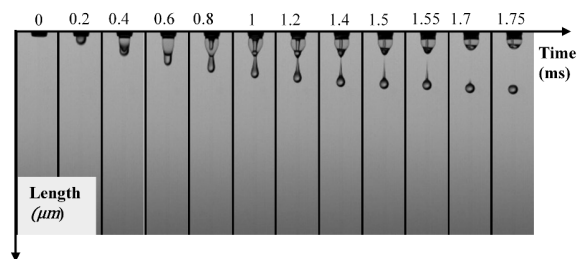

Fig. 11.   Droplet formation after hysteresis compensation at 100 Hz with PEDOT:PSS.
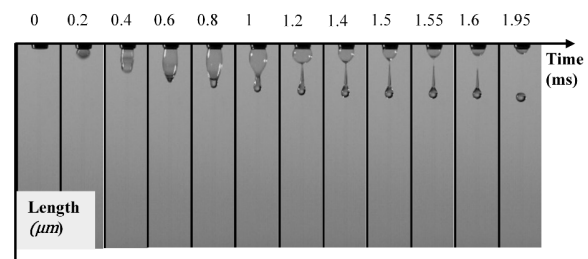

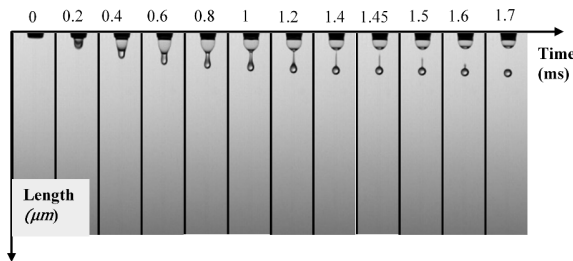Fig. 12.   Droplet formation at 100 Hz with silver nanoparticle ink.

Fig. 13. Droplet formation after compensation at 100 Hz with silver nanoparticle ink.

Table III summarizes the droplet formation evaluation for both cases at 100 Hz before and after hysteresis compensation, with a recording time set from 0 to 2.1 ms.

TABLE III. DROPLET FORMATION EVALUATION WITH PEDOT:PSS AND SILVER NANOPARTICLE INK AT 100 HZ.

Parameters	Before compensation	After compensation
PEDOT:PSS		
Droplet making time (ms)	1.7	1.2
Droplet diameter (μm)	228.68	212.2
Droplet volume (nL)	6.26	5
Breaking tail (μm)	378.57	168.29
Total tail (μm)	814.32	621.95
SILVER NANOPARTICLES		
Droplet making time (ms)	1.9	1.7
Droplet diameter (μm)	195.14	165.98
Droplet volume (nL)	3.89	2.39
Breaking tail (μm)	562.5	316.67
Total tail (μm)	845.06	540.05

Overall, the parameters at the frequency of 100 Hz are lower than those at 5 Hz in each category. Similarly, the effect after hysteresis compensation is lower than in the original state. The droplet making time at the frequency of 100 Hz is lower compared to that at 5 Hz, under the same experimental conditions. The value before compensation is about 2.15 ms, then decreased to 1.75 ms after compensation at the frequency of 5 Hz compared to the values of about 1.9 ms and 1.7 ms at the frequency of 100 Hz. The droplet diameter at the frequency of 5 Hz before compensation is about 210.54 μm, whereas after compensation it is 187.65 μm, which determines a droplet volume of around 4.89 nL and 3.46 nL, respectively. The values of the droplet diameter and droplet volume before and after compensation are 195.14 μm, 165.98 μm and 3.89 nL, 2.39 nL at the frequency of 100 Hz. The values of the breaking tail at the frequency of 5 Hz before compensation and after compensation are 525.05 μm, and 885.39 μm. Also the values of the total tail at 5 Hz are 420 μm and 877.5 μm. At the frequency of 100 Hz, the breaking tail before and after compensation is estimated at 562.5 μm and 316.67 μm, whereas the total tail has shown a big gap before and after compensation, which is recorded at 845.06 μm and 540.05 μm, in turn. Regarding the experiment with the silver nanoparticle ink, at the frequency of 5 Hz the tail length did not demonstrate a great difference before and after compensation.

IV. CONCLUSION

In this study, experimental hysteresis compensation is performed in a magnetostrictive inkjet print-head. An RC circuit is utilized at the frequencies of 5 Hz and 100 Hz. The results revealed that the capacitance value is disproportionate at a higher frequency gap. The optimal capacitance value at 5 Hz is approximately 10.75 μF and the Hysteresis Loss (HL) decreases to 16.62%, while at 100 Hz, this ratio is only 4.32% with a capacitance value of 335 μF. It is noted that the hysteresis loop at 5Hz is smaller than that at 100 Hz after compensation.

The findings exhibited that the above optimal capacitance value used in the inkjet printing system affected the droplet parameters, namely the droplet volume, time required for making droplets, droplet diameter breaking tail, and total tail, which decreased through the utilization of PEDOT:PSS and silver nanoparticle ink. This could be handled with a thin line of droplets on the surface allowing for the manufacturing of various substrates when utilizing a higher frequency. One method to decrease the tail length could be to reduce the flow rate, another one to decrease the input current, or optimize the capacitor. The current study presents a promising method applying the magnetostrictive actuator for controlling the droplet formation in the inkjet print-head. This compensation method could reduce the satellite effect when printing in a flexible circuit, such as a temperature sensor. However, the study focuses only on two frequencies which may generate certain limitations and challenges when dealing with other frequencies. Further studies could focus on a higher frequency to reduce HL by using the selected capacitor.

REFERENCES

[1] Y. Wu *et al.*, "Research progress on the application of inkjet printing technology combined with hydrogels," *Applied Materials Today*, vol. 36, Feb. 2024, Art. no. 102036, https://doi.org/10.1016/j.apmt.2023.102036.

[2] D. Zhao, H. Zhou, Y. Wang, J. Yin, and Y. Huang, "Drop-on-demand (DOD) inkjet dynamics of printing viscoelastic conductive ink," *Additive Manufacturing*, vol. 48, Dec. 2021, Art. no. 102451, https://doi.org/10.1016/j.addma.2021.102451.

[3] N. Sezer and M. Koç, "A comprehensive review on the state-of-the-art of piezoelectric energy harvesting," *Nano Energy*, vol. 80, Feb. 2021, Art. no. 105567, https://doi.org/10.1016/j.nanoen.2020.105567.

[4] A. Fujioka, S. Seo, T. Kanda, S. Wakimoto, and D. Yamaguchi, "A Microchannel Device for Droplet Classification by Manipulation Using Piezoelectric Vibrator," *Actuators*, vol. 13, no. 3, Mar. 2024, Art. no. 95, https://doi.org/10.3390/act13030095.

[5] S. Azizi Machekposhti, S. Mohaved, and R. J. Narayan, "Inkjet dispensing technologies: recent advances for novel drug discovery," *Expert Opinion on Drug Discovery*, vol. 14, no. 2, pp. 101–113, Feb. 2019, https://doi.org/10.1080/17460441.2019.1567489.

[6] B. Andò, S. Baglio, A. R. Bulsara, T. Emery, V. Marletta, and A. Pistorio, "Low-Cost Inkjet Printing Technology for the Rapid Prototyping of Transducers," *Sensors*, vol. 17, no. 4, Apr. 2017, Art. no. 748, https://doi.org/10.3390/s17040748.

[7] T. H. da Costa and J. W. Choi, "Low-cost and customizable inkjet printing for microelectrodes fabrication," *Micro and Nano Systems Letters*, vol. 8, no. 1, Jan. 2020, Art. no. 2, https://doi.org/10.1186/s40486-020-0104-7.

[8] O. Oktavianty, T. Kyotani, S. Haruyama, and K. Kaminishi, "New actuation waveform design of DoD inkjet printer for single and multi-drop ejection method," *Additive Manufacturing*, vol. 25, pp. 522–531, Jan. 2019, https://doi.org/10.1016/j.addma.2018.12.008.

[9] Y. W. Park, O. K. Oh, and M. D. Noh, "Ejection feasibility of high viscosity fluid with magnetostrictive inkjet printhead," *International Journal of Precision Engineering and Manufacturing*, vol. 16, no. 7, pp. 1369–1374, Jun. 2015, https://doi.org/10.1007/s12541-015-0180-4.

[10] F. C. Dezza, S. Cinquemani, M. Mauri, M. Maglio, and F. Resta, "A model of magnetostrictive actuators for active vibration control," in *2011 IEEE International Symposium on Industrial Electronics*, Jun. 2011, pp. 847–852, https://doi.org/10.1109/ISIE.2011.5984269.

[11] K. H. Choi *et al.*, "Electrode configuration effects on the electrification and voltage variation in an electrostatic inkjet printing head," *Journal of Micromechanics and Microengineering*, vol. 20, no. 7, Mar. 2010, Art. no. 075033, https://doi.org/10.1088/0960-1317/20/7/075033.

[12] X. Yang *et al.*, "An overview on the principle of inkjet printing technique and its application in micro-display for augmented/virtual realities," *Opto-Electronic Advances*, vol. 5, no. 6, Jun. 2022, Art. nop. 210123–24, https://doi.org/10.29026/oea.2022.210123.

[13] K. Yan, J. Li, L. Pan, and Y. Shi, "Inkjet printing for flexible and wearable electronics," *APL Materials*, vol. 8, no. 12, Dec. 2020, Art. no. 120705, https://doi.org/10.1063/5.0031669.

[14] K. S. Kwon, M. K. Rahman, T. H. Phung, S. D. Hoath, S. Jeong, and J. S. Kim, "Review of digital printing technologies for electronic materials," *Flexible and Printed Electronics*, vol. 5, no. 4, Sep. 2020, Art. no. 043003, https://doi.org/10.1088/2058-8585/abc8ca.

[15] T. Cao, Z. Yang, H. Zhang, and Y. Wang, "Inkjet printing quality improvement research progress: A review," *Heliyon*, vol. 10, no. 10, May 2024, https://doi.org/10.1016/j.heliyon.2024.e30163.

[16] M. A. Shah, D. G. Lee, B. Y. Lee, and S. Hur, "Classifications and Applications of Inkjet Printing Technology: A Review," *IEEE Access*, vol. 9, pp. 140079–140102, 2021, https://doi.org/10.1109/ACCESS.2021.3119219.

[17] G. Xue, Z. He, D. Li, Z. Yang, and Z. Zhao, "Analysis of the giant magnetostrictive actuator with strong bias magnetic field," *Journal of Magnetism and Magnetic Materials*, vol. 394, pp. 416–421, Nov. 2015, https://doi.org/10.1016/j.jmmm.2015.06.083.

[18] Y. Zhu, X. Yang, and N. M. Wereley, "Research on hysteresis loop considering the prestress effect and electrical input dynamics for a giant magnetostrictive actuator," *Smart Materials and Structures*, vol. 25, no. 8, Apr. 2016, Art. no. 085030, https://doi.org/10.1088/0964-1726/25/8/085030.

[19] K. Xiao, Z. Wang, H. Wang, J. Sun, Y. Zheng, and Y. Huang, "A precision-drive hysteresis model with an equal-density weight function for GMA feedforward compensation," *Nanotechnology and Precision Engineering*, vol. 6, no. 2, Mar. 2023, Art. no. 023002, https://doi.org/10.1063/10.0017659.

[20] K. G. Aktas and I. Esen, "State-Space Modeling and Active Vibration Control of Smart Flexible Cantilever Beam with the Use of Finite Element Method," *Engineering, Technology & Applied Science Research*, vol. 10, no. 6, pp. 6549–6556, Dec. 2020, https://doi.org/10.48084/etasr.3949.

[21] Q. T. Dao, V. V. Dinh, C. T. Vu, T. Q. Pham, and D. M. Duong, "An Adaptive Sliding Mode Controller for a PAM-based Actuator," *Engineering, Technology & Applied Science Research*, vol. 13, no. 1, pp. 10086–10092, Feb. 2023, https://doi.org/10.48084/etasr.5539.

[22] J. Zhao, Y. Li, Y. Cao, F. Zhang, M. Cui, and R. Xu, "High-Precision Position Tracking Control with a Hysteresis Observer Based on the Bouc–Wen Model for Smart Material-Actuated Systems," *Actuators*, vol. 13, no. 3, Mar. 2024, Art. no. 105, https://doi.org/10.3390/act13030105.

[23] Y. K. Al-Nadawi, X. Tan, and H. K. Khalil, "Inversion-Free Hysteresis Compensation via Adaptive Conditional Servomechanism With Application to Nanopositioning Control," *IEEE Transactions on Control Systems Technology*, vol. 29, no. 5, pp. 1922–1935, Sep. 2021, https://doi.org/10.1109/TCST.2020.3026018.

[24] Y. Yang, "Piezoelectric Actuators Application and Hysteresis Modelling: A Brief Survey," *Open Access Library Journal*, vol. 10, no. 8, pp. 1–36, Jul. 2023, https://doi.org/10.4236/oalib.1110482.

[25] N. Ahmed, P. J. Smith, and N. A. Morley, "Inkjet Printing Magnetostrictive Materials for Structural Health Monitoring of Carbon Fibre-Reinforced Polymer Composite," *Sensors*, vol. 24, no. 14, Jan. 2024, Art. no. 4657, https://doi.org/10.3390/s24144657.